Acta Crystallographica Section D
Biological Crystallography
ISSN 0907-4449

Structure of the inactive variant C60S of *Mycobacterium tuberculosis* thiol peroxidase

Matthias Stehr,[a] Hans Jürgen Hecht,[b]* Timo Jäger,[c]‡ Leopold Flohé[c]‡ and Mahavir Singh[a]*

[a]Department GNA, GBF – Gesellschaft für Biotechnologische Forschung, Mascheroder Weg 1, D-38124 Braunschweig, Germany, [b]Department SB, GBF – Gesellschaft für Biotechnologische Forschung, Mascheroder Weg 1, D-38124 Braunschweig, Germany, and [c]Department of Biochemistry, Technical University of Braunschweig, Mascheroder Weg 1, 38124 Braunschweig, Germany

‡ Present address: Molisa GmbH, Universitätsplatz 2, D-39106 Magdeburg, Germany.

Correspondence e-mail: hjh@gbf.de, msi@gbf.de

Received 22 November 2005
Accepted 6 March 2006

PDB Reference: *Mt*Tpx, 1y25, r1y25sf.

The genome of *Mycobacterium tuberculosis* encodes several peroxiredoxins (Prxs) thought to be active against organic and inorganic peroxides. The open reading frame Rv1932 encodes a 165-residue thiol peroxidase (Tpx), which belongs to the atypical 2-Cys peroxiredoxin family. The crystal structure of the C60S mutant of *M. tuberculosis* Tpx (*Mt*Tpx) crystallized in space group $P3_121$, with unit-cell parameters a = 106.08, b = 106.08, c = 65.33 Å. The structure has been refined to an R value of 17.1% (R_{free} = 24.9%) at 2.1 Å resolution. *Mt*Tpx is structurally homologous to other peroxiredoxins, including the mycobacterial AhpC and AhpE. The inactive *Mt*Tpx C60S mutant structure closely resembles the structure of *Streptococcus pneumoniae* Tpx (*Sp*Tpx) and thus represents the reduced enzyme state. The mutated active-site serine is electrostatically linked to Arg130 and hydrogen bonded to Thr57, practically identical to the cysteine in *Sp*Tpx. A cocrystallized acetate molecule mimics the position of the substrate and interacts with Ser60, Arg130 and Thr57.

1. Introduction

In the *Mycobacterium tuberculosis* (*Mt*) genome, several open reading frames have been identified encoding peroxiredoxins: two bcp-type peroxiredoxins [Rv1608c (bcpB) and Rv2521 (bcp)], one 1-Cys peroxiredoxin [Rv2238c (AhpE)] and two 2-Cys peroxiredoxins [Rv2428 (AhpC) and Rv1932 (Tpx)]. *Mt*Tpx has 165 residues and from sequence homology belongs to the subclass of bacterial atypical 2-Cys peroxiredoxins (Hofmann *et al.*, 2002; Choi *et al.*, 2003) with the peroxidatic N-terminal cysteine at residue 60 and the resolving cysteine at residue 93, in contrast to the mammalian typical 2-Cys peroxiredoxins, where the resolving cysteine is C-terminal. Homologous thiol peroxidases (Tpx) are widely distributed among eubacteria but do not occur in mammals. Detailed biochemical investigations have been carried out primarily on *Escherichia coli* Tpx, showing the enzyme to be involved in the thioredoxin-dependent oxidative stress response (Cha *et al.*, 1995), establishing a functional role for the second cysteine that is conserved in the subclass (Cha *et al.*, 1996) and the detailed kinetic mechanism (Baker & Poole, 2003). Structural studies on the *E. coli* enzyme have shown a disulfide bridge between the two functional cysteines in the fully oxidized form (Choi *et al.*, 2003; PDB code 1qxh), which was also found in the structure of the homologous enzyme from *Haemophilus influenzae* (PDB code 1q98, 2003). The structure of the Tpx from *Streptococcus pneumoniae* (PDB code 1psq, 2003) showed the enzyme in the fully reduced state and revealed large structural differences between the two states.

The mycobacterial antioxidant defence is linked to drug resistance and virulence *via* catalase (KatG) deficient resistance to the primary tuberculostatic isoniazid (INH; Sherman *et al.*, 1996). Loss of catalase makes the pathogenic bacteria more susceptible to the host's oxidative defence unless it is compensated by other components of the bacterial antioxidant defence, making the peroxiredoxins, which at least participate in the bacterial antioxidant defence, potential drug targets. Detailed biochemical investigations on mycobacterial peroxiredoxins have been carried out mainly on AhpC (Bryk *et al.*, 2000, 2002), but recently Jaeger *et al.* (2004) identified Tpx as more

Table 1
Data-collection and refinement statistics.

Values in parentheses are for the highest resolution shell.

Space group	$P3_121$
Unit-cell parameters (Å, °)	a = 106.089, b = 106.089, c = 65.334, α = 90.00, β = 90.00, γ = 120.00
Resolution limits (Å)	30.77–2.10
No. of unique reflections	23364
Completeness (%)	98.2 (97.0)
Data redundancy	3.5 (2.8)
$R_{\rm merge}$† (%)	4.8 (26.0)
$I/\sigma(I)$	19.7 (3.7)
$R_{\rm work}/R_{\rm free}$‡ (%)	17.1/24.9
R.m.s. bond lengths (Å)	0.024
R.m.s. bond angles (°)	2.3
No. of protein residues	330
No. of water molecules	368
No. of hetero molecules	2 (ACT)
Average B factor (Å^2)	30.8
Residues in Ramachandran plot regions (%)	
Most favoured	92.3
Additional allowed	7.7
Generously allowed	0.0

† $R_{\rm merge} = \sum_{\mathbf{h}}\sum_i[|I_i(\mathbf{h}) - \langle I(\mathbf{h})\rangle|]/\sum_{\mathbf{h}}\sum_i I_i(\mathbf{h})$, where $I_i(\mathbf{h})$ is the ith intensity measurement and $\langle I(\mathbf{h})\rangle$ is the weighted mean of all measurements of $I(\mathbf{h})$. ‡ $R_{\rm work}$ and $R_{\rm free} = \sum_h[|F(\mathbf{h})_o| - |F(\mathbf{h})_c|]/\sum_{\mathbf{h}}|F(\mathbf{h})_o|$, where $|F(\mathbf{h})_o|$ and $|F(\mathbf{h})_c|$ are the observed and calculated amplitudes, respectively. $R_{\rm free}$ was calculated using 5% of data.

efficient in protecting *M. tuberculosis* against oxidative and nitrosative stress. In order to establish a structural basis for potential inhibitor design of MtTpx, we decided to investigate the structure of the inactive C60S variant of the enzyme, reasoning that this variant would be representative for the fully reduced enzyme state and would avoid the potential crystallization problems caused by a mixture of structurally different reduced and oxidized forms.

2. Materials and methods

2.1. Protein expression and purification

The mutation C60S was introduced by site-directed mutagenesis PCR (Higuchi *et al.*, 1988) using the Tpx gene cloned into pET22b(+) as template (Jaeger *et al.*, 2004). The mismatched primers 5′-CACCGGTG**TCC**GCGACGAGTG-3′ (forward) and 5′-CACTCGTCG-C**GGA**CACCGGTG-3′ (reverse) were used. The triplet coding for the mutation is shown in bold.

The mutation was introduced with the forward mismatched primer in combination with the pET22b(+) T7 terminator primer (5′-GCTAGTTATTGCTCAGCGG-3′) and the reverse mismatched primer in combination with the pET22b(+) T7 promotor primer (5′-TAATACGACTCACTATAGGG-3′). Reaction mixtures contained 10–40 ng template DNA, 125 ng of each primer, 20 µ*M* dNTPs and 1 µl PfuTurbo Polymerase (Stratagene, La Jolla, USA). 30 cycles of 368 K for 30 s, 323 K for 60 s and 345 K for 1 min were carried out in a Biometra Cycler followed by 345 K for 10 min. Both resulting PCR products which carried the mutation were cut from a 1% agarose gel and purified with the QIAquick kit (Qiagen, Hilden, Germany). The relocation of the mutation was carried out in a PCR reaction that included both purified overlapping PCR products in combination with the T7 promotor and terminator primer. The purified PCR product was digested with *Nde*I and *Hin*dIII, ligated into the pET22b(+) vector (Novagen, Madison, USA) and subsequently transformed into *E. coli* BL21(DE3). The *Mt*Tpx DNA sequence was confirmed by DNA sequencing at the Department of Genome Analysis, GBF Braunschweig, Germany. The mutant protein was expressed and purified as described in Jaeger *et al.* (2004).

2.2. Crystallization, data collection, structure solution and refinement

Prior to crystallization, the protein was dialyzed against 20 m*M* Tris–HCl, 1 m*M* EDTA pH 7.4 buffer and concentrated to 8 mg ml^{-1}. Crystals were grown using the sitting-drop method at 292 K. 5 µl protein solution was mixed with 5 µl mother liquor (20% PEG 8000, 100 m*M* sodium cacodylate pH 6.5, 200 m*M* magnesium acetate) and equilibrated against 1 ml mother liquor. Crystals of dimensions 0.2 × 0.16 × 0.16 mm were obtained after 3–4 d. The crystals belong to the trigonal space group $P3_121$, subsequently proven to be correct by molecular replacement, with unit-cell parameters a = 106.08, b = 106.08, c = 65.33 Å. The asymmetric unit contains two molecules of *Mt*Tpx. Before transfer into a nitrogen-gas stream kept at 100 K, the crystals were washed for a few seconds in 20% PEG 8000, 100 m*M* sodium cacodylate pH 6.5, 200 m*M* magnesium acetate and 10% glycerol as cryoprotectant. Data were collected at λ = 1.5418 Å on a Rigaku rotating-anode generator with a Rigaku R-AXIS IV image-plate system to a resolution of 2.1 Å. The data set was processed with *MOSFLM* (Collaborative Computational Project, Number 4, 1994) and scaled with *SCALA* (Collaborative Computational Project, Number 4, 1994).

The structure of Tpx was solved by molecular replacement with the program *PHASER* (Collaborative Computational Project, Number 4, 1994) using a model of *Mt*Tpx generated with *MODELLER* v.6.1 (Sali & Blundell, 1993) from the structure of *S. pneumoniae* Tpx (PDB code 1psq) using default parameters and a sequence alignment obtained using *CLUSTALW* (Thompson *et al.*, 1994). The structure of *Mt*Tpx deposited with the PDB by the TB Structural Genomics Consortium (TBSGC; PDB code 1xvq, 2004) was not available at that time. Subsequent refinement was carried out with *REFMAC*5 (Murshudov *et al.*, 1997) with intermittent manual model correction using the program *O* (Jones *et al.*, 1991). NCS restraints were not thought necessary at the resolution used in the refinement. In the last stage of the refinement TLS parameters were introduced (Winn *et al.*, 2001) and water molecules were added using *ARP/wARP* (Collaborative Computational Project, Number 4, 1994) until R factors converged. The final R factors were 17.1% for reflections included in the refinement ($R_{\rm cryst}$) and 24.9% for 5% of all reflections excluded from refinement ($R_{\rm free}$) (Table 1). Superimpositions were calculated with *LSQMAN* (Sierk & Kleywegt, 2004) with a distance cutoff of 3.5 Å.

3. Results and discussion

The final model for Tpx comprises 2378 atoms for the two independent protein molecules in the asymmetric unit of the crystal together with 368 water molecules and two acetate molecules. Data-collection and refinement statistics including geometry analysis with *PROCHECK* (Collaborative Computational Project, Number 4, 1994) are compiled in Table 1. The two molecules in the asymmetric unit have nearly identical structures, with an r.m.s. deviation of 0.3 Å. The C^α atoms show no major conformational differences. Only a few side chains on the surface differ slightly in their conformation.

Topologically, the structure of *Mt*Tpx conforms to the structure of *E. coli* Tpx described by Choi *et al.* (2003) (PDB code 1qxh), indicated by an r.m.s. deviation of 1.0 Å for 132 C^α atoms with the exception of the vicinities of the peroxidatic and resolving cysteines. In these areas and in the overall structure, however, the structure of *Mt*Tpx is very similar to the structure of Tpx from *S. pneumoniae* (PDB code 1psq), with an r.m.s. deviation of 0.6 Å for 92 C^α atoms of the core of the molecule, including both cysteines. Large differences

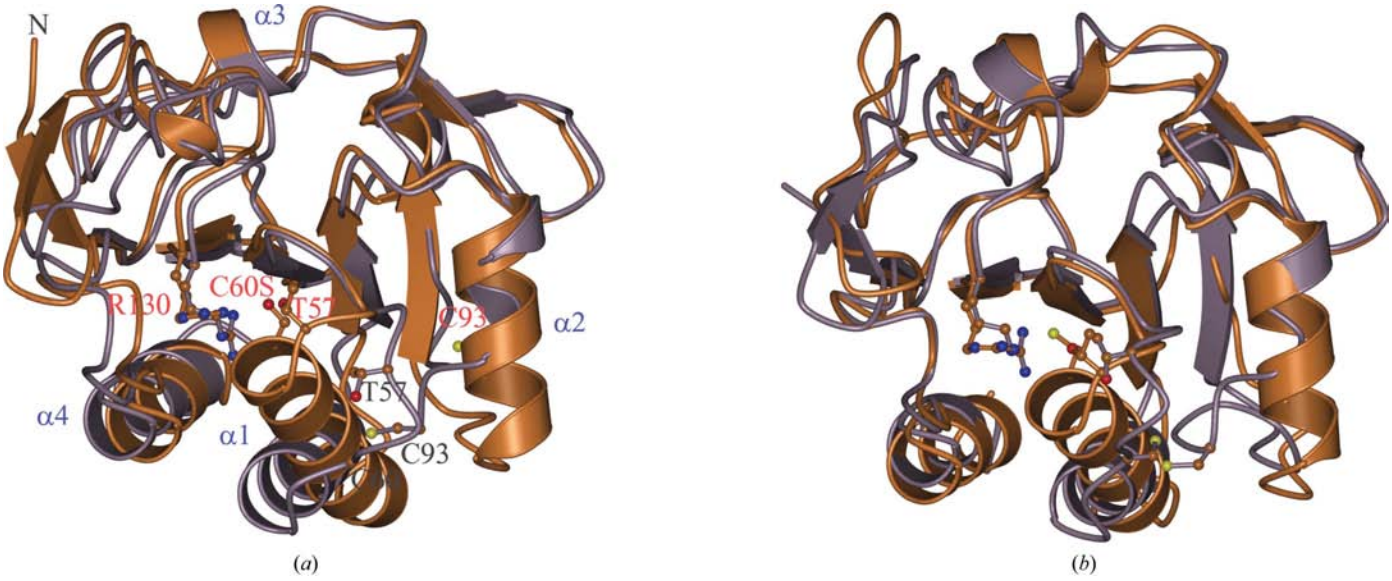

Figure 1
Superimposition of reduced and oxidized *Mt*Tpx (*a*) as represented by C60S *Mt*Tpx (brown; red residue labels) and *Mt*Tpx 1xvq (grey; black residue labels). Helices are labelled blue. For comparison, a superimposition of *Sp*Tpx 1PSQ (brown, reduced) and *Hi*Tpx 1Q89 (grey, oxidized) is shown in (*b*). This figure was drawn with *MOLSCRIPT* (Kraulis, 1991) and rendered with *PovRay*.

occur mainly near the N-terminus in the region of residues 12–23 and at the loop 71–77. The overall r.m.s. deviation for 154 C^{α} atoms common to both structures therefore is 1.2 Å. The vicinity of the active site, residues 56–62, is very similar in both structures, with an r.m.s. deviation of 1.0 Å for all 43 common atoms. The side-chain conformation of Ser60, which replaced the active cysteine, is identical to the cysteine in 1psq and even the side-chain conformations for Thr57 and Arg130, which activate the peroxidatic cysteine (Poole, 2005), are identical to 1psq, confirming that the inactive C60S variant is representative of the fully reduced state.

Compared with the structure of *Mt*Tpx deposited with the PDB by the TB Structural Genomics Consortium (TBSGC; PDB code 1xvq), the r.m.s. deviation of 124 C^{α} atoms is 0.9 Å. The vicinity of the peroxidatic cysteine Cys60, which is in the C60S variant part of the α1 helix (Fig. 1, residues 57–75), is in an extended conformation in 1xvq with the helix starting at residue 61. This area in 1xvq is very similar to the structures of *E. coli* Tpx 1qxh and *H. influenzae* Tpx 1q98, both of which are identified by the disulfide bridge between the peroxidatic and the resolving cysteine as being in the fully oxidized state. In 1xvq, however, coordinates for S^{γ} of Cys60 and the disulfide bridge to Cys93 are missing, although the C^{α} atoms of Cys60 and Cys93 are at a similar distance (5.4 Å) as in 1qxh (5.6 Å) and in 1q98 (6.4 Å). Loss of one S atom from a disulfide bridge has also been observed in acetylcholinesterase (Weik *et al.*, 2000) and was attributed to X-ray-induced formation of disulfide radicals (Weik *et al.*, 2002). Residues 94–99 are also missing in the coordinates of 1xvq, probably as a consequence of additional disorder induced by the radiation damage.

Therefore, taking 1xvq as representative of the fully oxidized state of *Mt*Tpx, a comparison shows the structural differences between the states to consist mainly of the partial unwinding of the helices α1 and α2 carrying the active cysteines. Helix α1 is additionally tilted and shifted by approximately 4 Å, which induces a similar shift of helix α4 (Fig. 1). Similar structural changes are visible in a comparison of *Sp*Tpx 1psq and *Hi*Tpx 1q98.

In the C60S *Mt*Tpx structure these regions do not show any indication of flexibility either in temperature factors or in quality of electron density and in *Sp*Tpx 1psq the temperature factors also do not indicate any flexibility of the regions affected by the structural changes, indicating that they are induced either by ligand binding or oxidation of the peroxidatic cysteine. The acetate molecule from the magnesium acetate additive to the crystallization buffer bound in the C60S *Mt*Tpx structure to C60S (Fig. 2) is evidently not sufficient to trigger conversion to the open conformation of the oxidized state.

The acetate forms strong hydrogen bonds from one of the carboxylate O atoms to the side chains of C60S, Thr57 and Arg130 as well as to the backbone nitrogen of C60S. This is practically identical to the carboxylate of the benzoate found in the structure of native human peroxiredoxin 5 (Declercq *et al.*, 2001; PDB code 1h4o) and

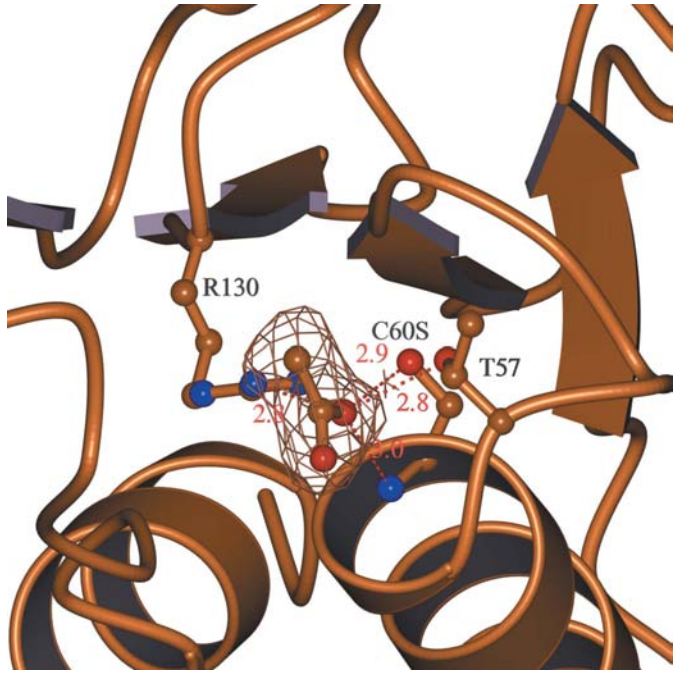

Figure 2
Active site of C60S *Mt*Tpx with bound acetate. The acetate is covered by electron density contoured at 1σ. Hydrogen-bonding distances (Å) are labelled in red. This figure was drawn with *MOLSCRIPT* (Kraulis, 1991) and rendered with *PovRay*.

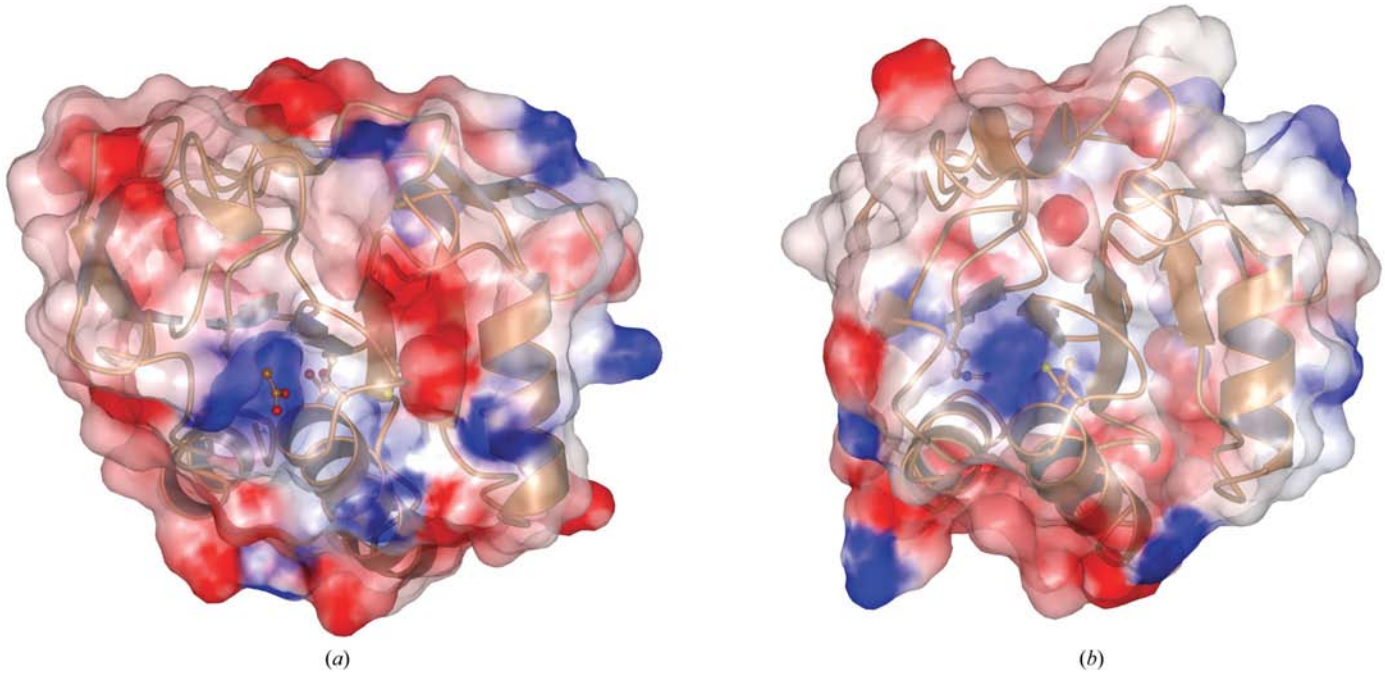

Figure 3
Electrostatic surfaces of C60S *Mt*Tpx (*a*) and *Mt*AhpE 1xxu (*b*). The electrostatic surface was calculated with *GRASP* (Nicholls *et al.*, 1991) using 0.1 *M* salt concentration and default parameters. The colour range is from $-10.0kT$ (red) to $+10.0kT$ (blue). This figure was drawn with *MOLSCRIPT* (Kraulis, 1991) and rendered with *PovRay*.

the methyl group of the acetate also forms similar hydrophobic contacts. In 1h4o, however, the source of the benzoate was unclear, as it was not a component of the crystallization buffer or the purification procedure (Declercq *et al.*, 2001).

Similar contacts are possible for the main substrates, hydrogen peroxide, *t*-butyl hydroperoxide and cumene hydroperoxide, identified by Jaeger *et al.* (2004) and the active-site pocket (Fig. 3) could easily accommodate the bulkier hydrophobic parts of the substrates. The low activity found by Jaeger *et al.* (2004) for linoleic acid hydroperoxide and phosphatidylcholin hydroperoxide is less understandable as preliminary modelling shows that the peroxo groups still should be able to reach the active-site cysteine.

Recently, the structures of two other mycobacterial peroxiredoxins, *Mt*AhpC (Guimaraes *et al.*, 2005; PDB code 2bmx) and *Mt*AhpE (Li *et al.*, 2005; PDB code 1xvw and 1xxu), have been reported. A superimposition of *Mt*Tpx with 2bmx gives an r.m.s. distance of 1.6 Å for 127 C^{α} atoms, but the structure shows the molecule to be in an intermediate state between the conformations of the reduced and oxidized state (Guimaraes *et al.*, 2005) and a comparison of the active sites in either state therefore is not possible. For the 1-Cys peroxiredoxin *Mt*AhpE, 138 C^{α} atoms of the molecule in the reduced state (1xxu) can be superimposed with an r.m.s. distance of 1.3 Å and 140 C^{α} atoms of the molecule in the oxidized state (1xvw). The vicinity of the active site, residues 56–62 in C60S *Mt*Tpx, is very similar in 1xxu, indicated by an r.m.s. difference of 1.1 Å for all 38 atoms of the corresponding residues, with the side-chain conformations for the active-site cysteine and the activating threonine and arginine identical to those in the C60S *Mt*Tpx structure. The active-site pocket in reduced *Mt*AhpE therefore is quite similar to C60S *Mt*Tpx (Fig. 3), including the apparent affinity for negatively charged ligands as indicated by the electrostatic surfaces and the bound acetate in the C60S *Mt*Tpx structure.

The quaternary structure of peroxiredoxins is dependent on subtype and redox state and for the prototype bacterial *E. coli* thiol peroxidase 1qxh a dimer has been reported for the oxidized state (Choi *et al.*, 2003). The two molecules in the asymmetric unit of C60S *Mt*Tpx are each part of dimers generated by the crystallographic twofold axis and a superimposition shows the dimers to be identical to the *Ec*Tpx dimer. Oxidized *Mt*Tpx 1xvq has one molecule in the asymmetric unit which is completed by crystallographic symmetry to form the same dimer, indicating that for this subtype of 2-Cys peroxiredoxins the dimeric state as described for *Ec*Tpx is not influenced by the redox state.

4. Conclusion

The inactive C60S variant of the mycobacterial thiol peroxidase Rv1932 closely resembles other bacterial atypical 2-Cys peroxiredoxins, first described by Choi *et al.* (2003) in detail for the *E. coli* enzyme in the oxidized state, and in particular is very similar in the vicinity of the active site to the structure of *S. pneumoniae* Tpx (PDB code 1psq), which is in the reduced state. The acetate bound to C60S, closely similar to the benzoate observed in human peroxiredoxin 5 (Declercq *et al.*, 2001), suggests an affinity for acidic ligands that is common to various types of peroxiredoxin. Considering in addition the geometric similarity of the active sites in the reduced state, in which most of the contacts to a ligand are formed by the absolutely conserved cysteine, threonine and arginine, the design of specific inhibitors may be problematic.

We would like to thank Sandra Berger for technical assistance during crystallization experiments. This work received financial support from the European Commission, grant QLK2-CT-2002-01682.

References

Baker, L. M. & Poole, L. B. (2003). *J. Biol. Chem.* **278**, 9203–9211.
Bryk, R., Griffin, P. & Nathan, C. (2000). *Nature (London)*, **407**, 211–215.

Bryk, R., Lima, C. D., Erdjument-Bromage, H., Tempst, P. & Nathan, C. (2002). *Science*, **295**, 1073–1077.
Cha, M. K., Kim, H. K. & Kim, I. H. (1995). *J. Biol. Chem.* **270**, 28635–28641.
Cha, M. K., Kim, H. K. & Kim, I. H. (1996). *J. Bacteriol.* **178**, 5610–5614.
Choi, J., Choi, S., Choi, J., Cha, M. K., Kim, I. H. & Shin, W. (2003). *J. Biol. Chem.* **278**, 49478–49486.
Collaborative Computational Project, Number 4 (1994). *Acta Cryst.* D**50**, 760–763.
Declercq, J. P., Evrard, C., Clippe, A., Stricht, D. V., Bernard, A. & Knoops, B. (2001). *J. Mol. Biol.* **311**, 751–759.
Guimaraes, B. G., Souchon, H., Honore, N., Saint-Joanis, B., Brosch, R., Shepard, W., Cole, S. T. & Alzari, P. M. (2005). *J. Biol. Chem.* **280**, 25735–25742.
Higuchi, R., Krummel, B. & Saiki, R. K. (1988). *Nucleic Acids Res.* **16**, 7351–7367.
Hofmann, B., Hecht, H. J. & Flohe, L. (2002). *Biol. Chem.* **383**, 347–364.
Jaeger, T., Budde, H., Flohe, L., Menge, U., Singh, M., Trujillo, M. & Radi, R. (2004). *Arch. Biochem. Biophys.* **423**, 182–191.
Jones, T. A., Zou, J.-Y., Cowan, S. W. & Kjeldgaard, M. (1991). *Acta Cryst.* A**47**, 110–119.
Kraulis, P. J. (1991). *J. Appl. Cryst.* **24**, 946–950.
Li, S., Peterson, N. A., Kim, M. Y., Kim, C. Y., Hung, L. W., Yu, M., Lekin, T., Segelke, B. W., Lott, J. S. & Baker, E. N. (2005). *J. Mol. Biol.* **346**, 1035–1046.
Murshudov, G. N., Vagin, A. A. & Dodson, E. J. (1997). *Acta Cryst.* D**53**, 240–255.
Nicholls, A., Sharp, K. A. & Honig, B. (1991). *Proteins*, **11**, 281–296.
Poole, L. B. (2005). *Arch. Biochem. Biophys.* **433**, 240–254.
Sali, A. & Blundell, T. L. (1993). *J. Mol. Biol.* **234**, 779–815.
Sherman, D. R., Mdluli, K., Hickey, M. J., Arain, T. M., Morris, S. L., Barry, C. E. III & Stover, C. K. (1996). *Science*, **272**, 1641–1643.
Sierk, M. L. & Kleywegt, G. J. (2004). *Structure*, **12**, 2103–2111.
Thompson, J. D., Higgins, D. G. & Gibson, T. J. (1994). *Nucleic Acids Res.* **22**, 4673–4680.
Weik, M., Berges, J., Raves, M. L., Gros, P., McSweeney, S., Silman, I., Sussman, J. L., Houee-Levin, C. & Ravelli, R. B. (2002). *J. Synchrotron Rad.* **9**, 342–346.
Weik, M., Ravelli, R. B., Kryger, G., McSweeney, S., Raves, M. L., Harel, M., Gros, P., Silman, I., Kroon, J. & Sussman, J. L. (2000). *Proc. Natl Acad. Sci. USA*, **97**, 623–628.
Winn, M. D., Isupov, M. N. & Murshudov, G. N. (2001). *Acta Cryst.* D**57**, 122–133.